

Coherent Dynamics in Solutions of Colloidal Plexcitonic Nanohybrids at Room Temperature

Nicola Peruffo, Fabrizio Mancin, and Elisabetta Collini*

The increasing ability to prepare systems with nanoscale resolution and address their optical properties with ultrashort time precision is revealing quantum phenomena with tremendous potential in quantum nanotechnologies. Colloidal plexcitonic materials promise to play a pivotal role in this scenario. Plexcitons are hybrid states originating from the mixing of the plasmon resonances of metal nanostructures with molecular excitons. They allow nanoscale confinement of electromagnetic fields and the establishment of strong couplings between light and matter, potentially giving rise to controllable and tunable coherent phenomena. However, the characterization of the ultrafast coherent and incoherent dynamics of colloidal plexciton nanohybrids remains highly unexplored. Here, two dimensional electronic spectroscopy (2DES) is employed to study the quantum coherent interactions active after the photoexcitation of these systems. By comparing the response of the nanohybrids with the one of the uncoupled systems, the nonlinear photophysical processes at the base of the coherent dynamics are identified, allowing a step forward toward the effective understanding and exploitation of these nanomaterials.

fulfilled by polaritonic materials. Polaritons result from the resonance coupling between electromagnetic waves and elementary excitations; and therefore, they can be defined as half-light half-matter coherent states.^[1] Typical representatives of these coherent superposition states are polaritons formed by quantum hybridization of molecular excitons and microcavity photons, for which several observations of nonlinear collective quantum effects are available.^[2] Nonetheless, these structures often require sophisticated and expensive fabrication techniques and specific geometries for their optical characterization.^[3,4] An attractive alternative strategy is to use colloidal plasmonic nanoparticles, which are tunable, scalable, and easy to synthesize by cheap wet chemistry methodologies.^[5–8] They can promote strong interactions with other photonic elements in close proximity, such as molecules or aggregates of molecules by confining electromagnetic fields to regions well below the diffraction

limit. Also in this case, the coupling leads to the formation of polariton hybrid states, called more specifically plexcitons, because they originate from the mixing of the plasmon resonance of the metal nanostructure with molecular excitons (**Figure 1a**).^[9,10]


A promising route to unlock the full potential of these hybrid materials for quantum-nano-photonics applications is the combination with ultrafast spectroscopy.^[12] Ultrafast time-domain optical studies can reveal how the coupling between plasmonic and molecular moieties results in new photophysical and dynamical properties, including new attractive nonlinearities and coherent quantum mechanical phenomena.^[13] These hold great promises not only in terms of advancements of fundamental knowledge, that is, to unveil still unexplored aspects of the light–matter and many-body interactions but also in view of possible frontier applications in the lively field of quantum technologies, including quantum information and functional quantum circuits.^[14] Particularly interesting in this context is the recent demonstration of measurable coherent interactions in the IR range for microcavity polariton materials^[15,16] and in the Vis range for plexcitonic nanoslit arrays.^[17] Considering the wide range of rich physics potentially emerging from these interactions, verifying to what extent the same kind of nonlinear phenomena can also be characterized in colloidal plexcitonic materials is of pivotal importance for effectively exploiting the new class of nanomaterials.

1. Introduction

The prospect of controlling light–matter interaction at the nanoscale and at the quantum–mechanical level is currently one of the most intriguing topics at the boundaries of nanotechnology, quantum technology, and photonics. This task is excellently

N. Peruffo^[†], F. Mancin, E. Collini
Department of Chemical Sciences
University of Padova
via Marzolo 1, 35131 Padova, Italy
E-mail: elisabetta.collini@unipd.it

E. Collini
Padua Quantum Technologies Research Center
Padova Italy

 The ORCID identification number(s) for the author(s) of this article can be found under <https://doi.org/10.1002/adom.202203010>

[†] Present address: Department of Chemistry and Molecular Biology, University of Gothenburg, Gothenburg 412 96, Sweden.

© 2023 The Authors. Advanced Optical Materials published by Wiley-VCH GmbH. This is an open access article under the terms of the Creative Commons Attribution-NonCommercial-NoDerivs License, which permits use and distribution in any medium, provided the original work is properly cited, the use is non-commercial and no modifications or adaptations are made.

DOI: 10.1002/adom.202203010

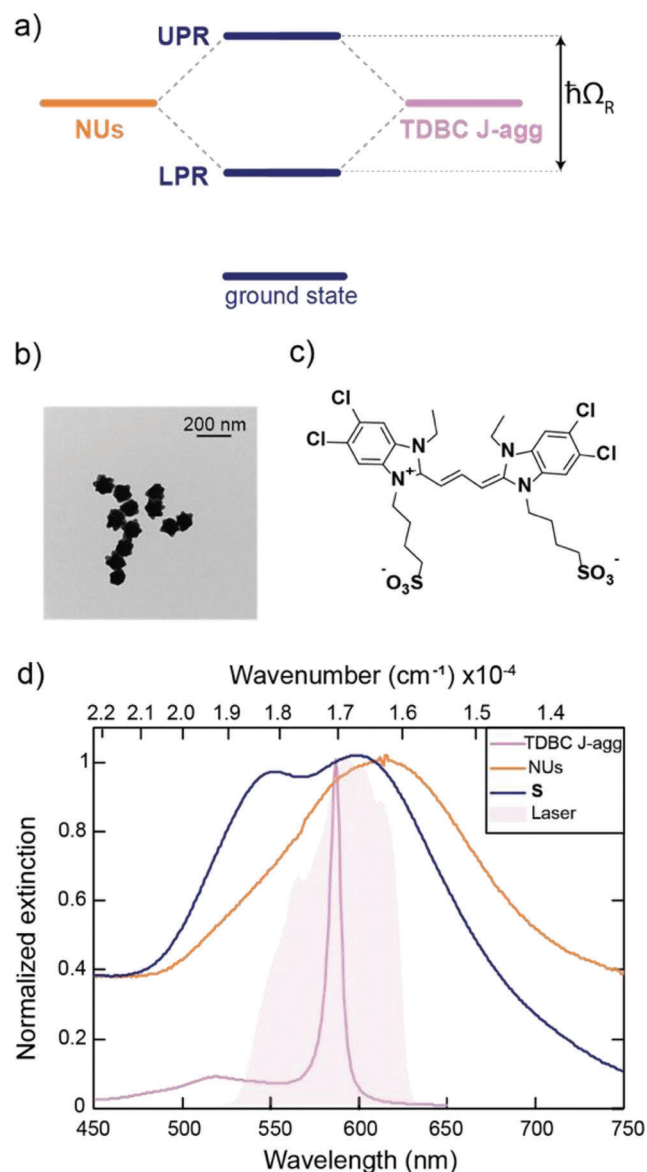


Figure 1. a) Scheme of the coupling between a plasmon resonance and an exciton transition to form two plexciton resonances (UPR and LPR) separated by the energy associated with the Rabi splitting ($\hbar\Omega_R$). b) TEM image of citrate-capped NUs (scalebar: 200 nm) with an average diameter of (82 ± 6) nm. c) Molecular structure of the TDBC molecule. d) Normalized extinction spectra of the nano hybrids (blue) and their constituents: NUs (orange) and TDBC J-aggregates (pink). The tip plasmon of bare NUs is centered at 610 nm ($16\,390\text{ cm}^{-1}$). The functionalization of the surface with TDBC induces the etching of the tips and a consequent plasmon blueshift.^[5] This is a favorable effect because it brings the plasmon resonance close to TDBC J-aggregates excitonic peak ($587\text{ nm} = 17\,035\text{ cm}^{-1}$), leading to a more effective resonance condition.^[11] The laser profile used for 2DES measurements is represented as a pink area.

In fact, resolving coherent dynamics in colloidal plexciton materials is a challenging task that has not already been reported. In general, the literature about their dynamics in the sub-100 fs is scarce,^[18–20] (even if the interest in their ultrafast dynamics is very high; see for instance refs. [21–24]). The main difficulty arises from the intrinsic nature of these samples: the con-

stituent plasmon nanoparticles are characterized by high dissipation rates and inhomogeneous broadening, which might result in a shortening of the observed ensemble coherences and call for a very demanding time resolution.^[25]

To fill this gap, in this work, we employed 2DES. The intrinsic multidimensionality of the response provided by 2DES was revealed to be particularly powerful to study many-body properties in semiconductor materials^[26,27] and, in general, to investigate coherent couplings in artificial nanomaterials and nanodevices toward quantum technology applications.^[28,29] Using this approach, experimental 2DES data on strongly coupled plexciton nano hybrids were collected and compared with the response of the uncoupled components. The results revealed clear experimental signatures of coherent dynamics.

2. Results and Discussion

2.1. Design and Linear Characterization of the Nano hybrids

The nano hybrids under investigation were prepared through colloidal chemistry methodologies by functionalizing citrate-capped gold nanourchins (NUs, Figure S1, Supporting Information), acting as plasmonic moieties, with cyanine dyes (TDBC) in the J-aggregate form, working as the excitonic medium (Figure 1b,c).^[30] Details on the preparation procedure are reported in the Section “Experimental Section” below. The nature of supramolecular forces promoting the nano hybrids formation, the estimation of the coupling regime, and its dependence on TDBC concentration and on the capping layer were thoroughly investigated in a previous publication.^[5] The choice of NUs has two main advantages: first, the tip plasmon is easily tunable by controlling the synthetic conditions, and this guarantees an adequate overlap with the dyes’ absorption;^[31] second, the NU structure features strong electric fields at the tips, which should positively contribute to the establishment of strong couplings.^[32] On the other side, NUs intrinsically present size and shape distributions, and this leads to inhomogeneously broadened bands that slightly complicate the estimate of the Rabi splitting and coupling regime, as discussed below.

In Figure 1d, the extinction spectrum of the nano hybrids (blue) is compared with the ones of pristine NUs (orange) and TDBC aggregates (pink). The spectrum of pristine NUs appears slightly redshifted than after the functionalization with TDBC. This phenomenon is due to the smoothing of the tips after the functionalization with the dye that exchanges citrate molecules on the NU surface. In this way, the direct interaction of TDBC molecules with the metal surface is promoted, which favors the coupling of the two moieties.^[5]

The appearance of two energy branches in the nano hybrids spectrum, namely the upper and lower plexciton branches, demonstrates a clear anti-crossing behavior near the position of the TDBC J-aggregate exciton resonance, indicating the effective activation of plasmon-exciton hybridization. Additional evidence was provided by the observation that the energy gap between the two peaks depends on the dye concentration.^[5] Indeed, when different samples with decreased dye concentration were characterized, we observed smaller energy gaps between the bands (see Note S3, Supporting Information). This behavior is typical evidence for the formation of plexcitons, where the Rabi splitting is

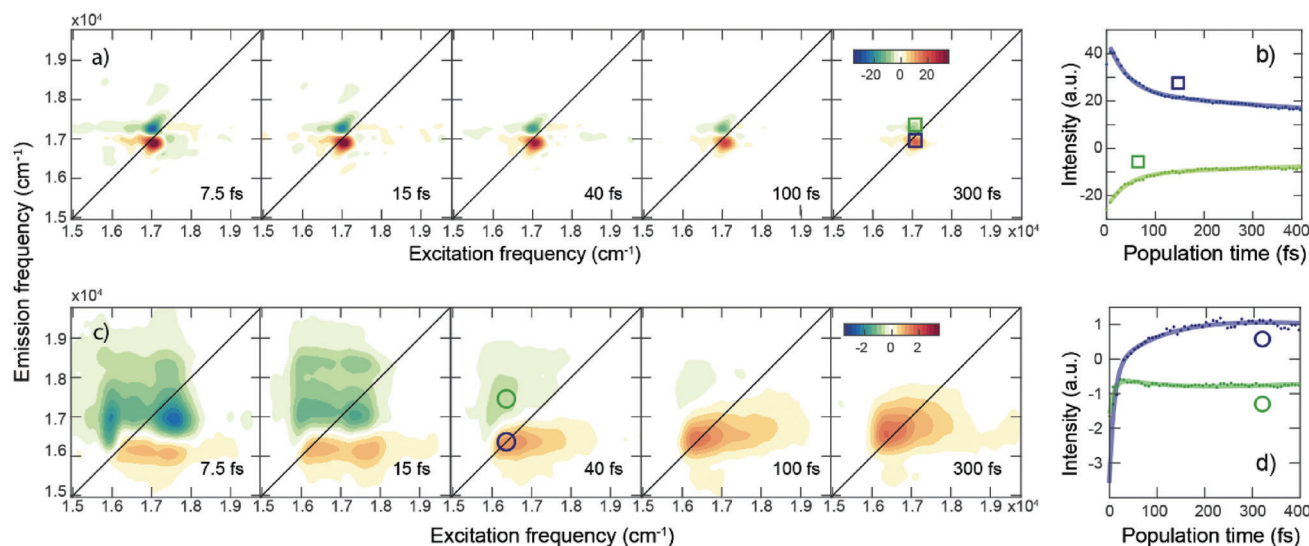


Figure 2. 2DES response of the uncoupled components: a,b) TDBC J-aggregates and c,d) NUs. Purely absorptive 2DES maps for TDBC J-aggregates at selected values of population time (a). Signal decay extracted at diagonal coordinates (17 040, 17 040 cm^{-1}), blue square, and at coordinates (17 040, 17 300 cm^{-1}), green square (b). Purely absorptive 2DES maps for NUs at selected values of population time. Signal decays extracted at diagonal coordinates (16 380, 16 380 cm^{-1}), blue circle, and at off-diagonal coordinates (16 380, 17 240 cm^{-1}) (c), green circle (d).

expected to be proportional to the square of the number of coupled molecules.

In the sample of Figure 1, the upper plexcitonic resonance (UPR) falls at 548 nm (18 250 cm^{-1}) and the lower plexcitonic resonance (LPR) falls at 602 nm (16 600 cm^{-1}). The Rabi splitting (Ω_R), calculated as the difference in frequency among the two resonances, is 1510 cm^{-1} . The magnitude of Ω_R provides a metric of the coupling strength between plasmonic nanoparticles and dye molecules.^[10,33,11] While the identification of the coupling regime based on experimental parameters is not quite universal;^[10,34,35] here, we consider that the conditions for strong coupling are achieved when $2\Omega_R > \gamma_{\text{TDBC}} + \gamma_{\text{NUs}}$, which has been shown to be the most restrictive threshold proposed for determining the strong coupling.^[10,36] γ_{TDBC} and γ_{NUs} are the associated amplitude decay rates of TDBC J-aggregates and NUs, quantified as spectral widths (full-width-at-half-maximum) of the extinction bands, as reported in Table S1, Supporting Information.^[3]

Note that because of intrinsic NUs' size and shape distributions, the full-width-at-half-maximum of the extinction spectrum overestimates the γ_{NUs} parameter, which may in turn lead to an underestimation of the coupling regime.^[37] Notwithstanding, the abovementioned condition for the formation of hybrid plexciton states in the investigated nanohybrids remains strictly valid. This is a crucial point for the interpretation of the photophysical behavior of nanohybrids. Indeed, although the NUs' size and shape distributions inevitably give rise also to a distribution of different nanohybrids with slightly different structures and couplings, the linear and nonlinear optical properties will be dictated by the fulfilled average condition of strong coupling.

In order to identify more clearly the possible role played by the excitonic and the plasmonic components in the plexciton nonlinearity, 2DES measurements were performed on suspensions of nanohybrids in water and compared with the 2DES response of the uncoupled constituents, that is, TDBC J-aggregates and NUs suspensions in water, all measured in the same conditions.

The spectral pulse profile was chosen to excite UPR and LPR simultaneously (Figure 1d). As we were mainly interested in investigating the ultrafast coherent behavior, we focused on a time window of 400 fs after photoexcitation. Details on the experimental technique are reported in the "Experimental Section" section below.

2.2. Ultrafast Dynamics of the Uncoupled Systems

Figure 2 summarizes the purely absorptive 2DES response of the uncoupled systems. Additional rephasing and non-rephasing 2DES maps are reported in Figures S2 and S3, Supporting Information. For the uncoupled systems and also for the plexciton nanohybrids below, the 2DES response is compared with previous results mainly obtained by pump-probe spectroscopy. In making this comparison, it is necessary to remember that the 2DES spectrum is typically expressed in electric field units, contrary to pump-probe spectra that are described in optical density units.^[38,39] This means that the signs of the 2DES and pump-probe signals are opposite. For example, photoinduced absorption phenomena appear as positive features in the pump-probe spectra and negative signals (blue-green color) in the 2DES spectra.

Figure 2a shows examples of purely absorptive 2DES maps at selected values of population time for TDBC J-aggregates in water. The obtained data agree with the results of previous investigations on the same system and show a dynamic behavior not particularly rich in the investigated timescale.^[20,40,41] The main feature appearing in the maps is a positive diagonal peak at 17 040 cm^{-1} , composed of contributions from bleaching and stimulated emission of the J band also dominating the linear absorption spectrum. In addition, a negative photoinduced absorption peak is found at slightly blueshifted emission frequencies, which is due to transitions from the one- to the two-exciton bands, as al-

ready indicated by previous pump-probe measurements.^[40] More details on the transitions giving rise to the signal distribution in the 2DES maps of TDBC J-aggregates are reported in Note S1, Supporting Information.

A global multiexponential fitting analysis^[42] (see Note S2, Supporting Information) was employed to quantify the kinetic constants regulating the relaxation dynamics. We identified short (40 fs) and long (>400 fs) non-oscillating decaying components (Figure S8, Supporting Information) that, in agreement with previous ultrafast experiments,^[20,43,44] have been attributed to dephasing by exciton phonon scattering and to slower deactivation processes (including exciton–exciton annihilation and relaxation to the ground state), respectively.^[45,40] No relevant oscillating components were detected, as clearly emerging from the time traces reported in Figure 2b.

Figure 2c reports the 2DES response of a suspension of NUs at various population times. The dynamics of nanoparticles are more complex and reflect the different equilibration steps of the nonequilibrium electron gas generated after the plasmon-resonant excitation.^[20,46–48] This electron gas equilibrates through a series of sequential steps that span the femtosecond to picosecond time scales, including ultrafast electronic plasmon dephasing, electron–electron scattering, electron–phonon scattering, and energy dissipation to the nanoparticle surroundings over tens to hundreds of picoseconds. While the ultrafast dynamics of several kinds of plasmonic nanoparticles have been extensively studied in the past decades by transient absorption experiments,^[47] less numerous are the characterizations by 2DES,^[20,49] and the maps in Figure 2c represent the first example of this technique applied to NUs.

As for J-aggregates, the 2DES response of NUs was analyzed by the same global multiexponential fitting analysis, which revealed that the NUs dynamics are dominated by three time constants of ≤ 10 fs, 125 fs, and $\gg 400$ fs (Figure S9, Supporting Information). At early times ($t_2 \approx 50$ fs), the signal distribution presents a complex pattern whose time evolution is dominated by the shortest time constant identified by the global fitting (≤ 10 fs). In previous works,^[20,50] such a time window was intentionally excluded from the analysis because it includes a wealth of different phenomena developing in a timescale comparable with the pulse duration and hardly distinguishable, including scattering, pulse overlap effects, induced polarization decay, Landau damping, wavevector randomization, transient grating, and plasmon dephasing.^[20,49,50] While the presence of any of these effects cannot be excluded, the peculiar signal distribution in the 2DES maps at early times and the DAS relative to the shortest time constant (Figure S9, Supporting Information) seem to suggest that the strongest contribution in our data might come from the dephasing of the hybridized core and tip plasmons of the NUs, lasting no longer than the pulse duration and instantaneously damped (see Note S1, Supporting Information). The challenging nature of the dynamics in this time range calls however for more targeted additional measurements.

For population times > 50 fs, the 2DES maps are dominated by a positive peak appearing on the diagonal (and below it) and a weaker negative peak appearing at higher values of the emission frequency. According to the signal distribution in the DAS plots (Figure S9, Supporting Information) and as exemplified by the time traces in Figure 2d, the intensity of the positive diagonal

peak first increases (with a kinetic quantified by the 125 fs time constant) and then decays in a timescale longer than the investigated time window ($\gg 400$ fs). This trend agrees with previous ultrafast measurements^[20,22,46–52] and closely resembles the 2DES behavior recorded for gold nanorods' suspensions.^[49] This peculiar signal distribution arises from spectral broadening and redshift of the plasmon resonance caused by the ultrafast electron heating consequent to photoexcitation.^[22,48,51–53]

Overall, the dephasing of the plasmon resonance (≤ 10 fs) generates excited electrons that are spread over different levels in the conduction band. These excited electrons rapidly equilibrate via electron–electron scattering to create a hot electron distribution (125 fs). The hot electron distribution then relaxes via phonon emission on a longer time scale, typical of a few picoseconds ($\gg 400$ fs).

2.3. Ultrafast Dynamics of Plexcitonic Nanohybrids

2.3.1. Population Dynamics

The results of the 2DES characterization of nanohybrids are summarized in **Figure 3**. The main features appearing in the spectra are two diagonal peaks at coordinates $16\,200\text{ cm}^{-1}$ and $17\,900\text{ cm}^{-1}$ (purple and orange circle, respectively, in Figure 3a) and two off-diagonal peaks at the associated cross coordinates (cyan and black circles). The position of these peaks, their amplitude and sign, and the associated dynamics are utterly distinct from the ones recorded in the 2DES maps of bare J-aggregates and NUs (Figure 2), indicating that the contribution of uncoupled moieties is negligible in the nanohybrids' response.

Let's focus our attention first on the diagonal peaks. The coordinates of the diagonal peaks correspond, within the approximation due to the convolution with the laser spectral profile, to the two plexciton resonances already identified in the extinction spectrum; and therefore, these signals can be attributed to nonlinearities involving the UPR and LPR, respectively. These peaks have an almost circular shape, typically associated with homogeneous broadening phenomena.^[54] This might indicate the presence of “motional narrowing,” a mechanism typically associated with the reduction of spectral linewidths in disordered systems by some averaging process. This mechanism has been invoked for many decades in many examples of strongly coupled systems, including molecular aggregates,^[55,56] polaritonic quantum well,^[57,58] and polaritonic planar cavities,^[18] but it is here observed for the first time in colloidal plexcitonic materials. Further measurements would be necessary to fully support this interpretation and provide more specific microscopic details of the effective mechanisms at play. Nonetheless, this evidence is particularly promising in assessing the overall coherent behavior of these materials because, as for cavity polaritons, it is expected that the establishment of this motional narrowing regime might be advantageous for preserving coherent interactions.^[57]

A closer look at the maps in Figure 3a also reveals that the diagonal peak corresponding to LPR progressively blue shifts. Similarly, UPR undergoes a redshift; although, less marked. Figure 3b reports the difference between the central values of the emission frequency (γ coordinate) of the two peaks as a function of the population time. This difference depends on the Rabi splitting

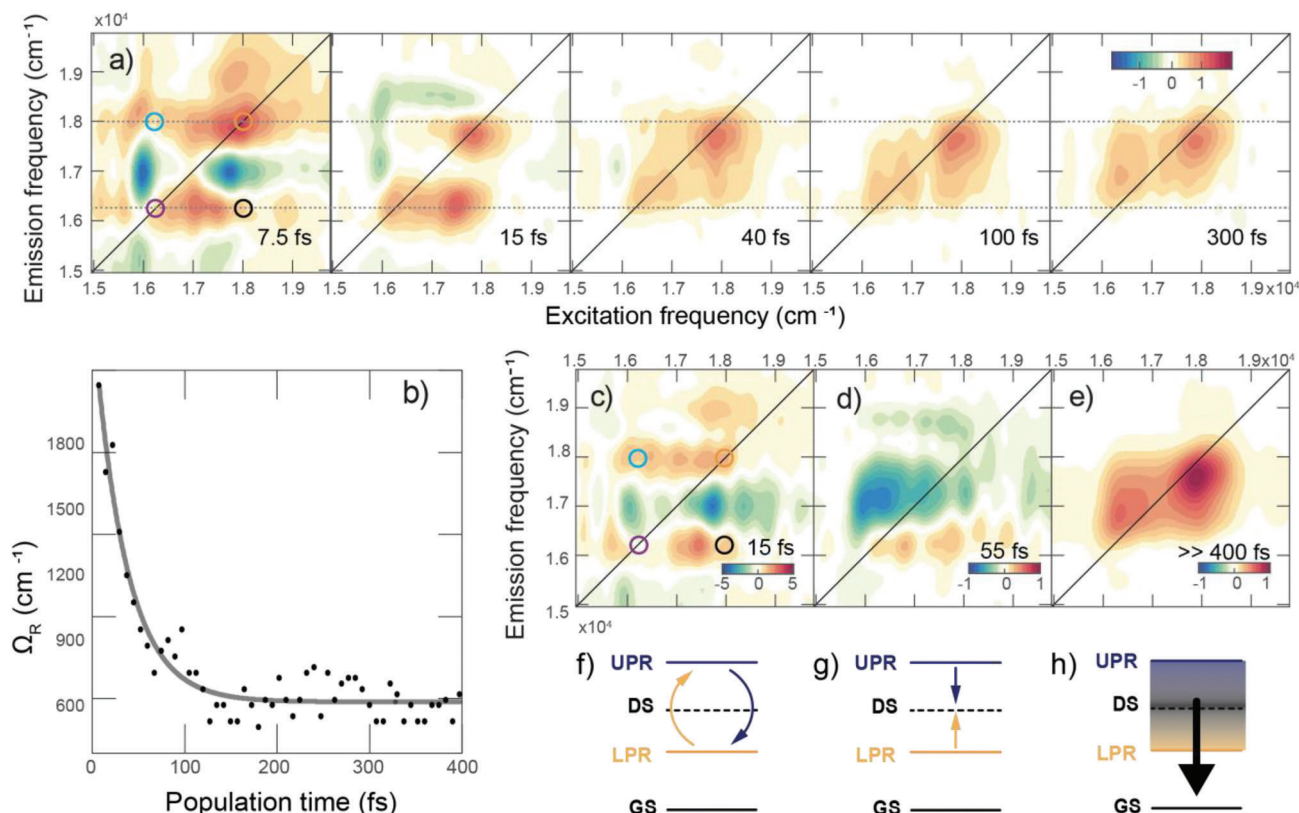


Figure 3. 2DES response of the nanohybrids. a) Purely absorptive 2DES maps at selected values of population time t_2 (normalized color scale). b) Time dependence of the experimental Rabi splitting estimated as the difference between the maxima of the UPR and LPR diagonal peaks (pinpointed by the orange and purple circles, respectively). The dots and the solid line represent the experimental points and the fitting curve, respectively. c–e) 2D-DAS associated with the three kinetic constants (values reported at the bottom) identified by the global fitting. f–h) Pictorial representation of the relaxation processes associated with the 2D-DAS (UPR = upper plexcitonic resonance, LPR = lower plexcitonic resonance, DS = dark states, and GS = ground state).

Ω_R , which directly monitors the coupling strength between plasmon and exciton. Therefore, the temporal evolution of Ω_R can be utilized to gain information on the dynamics of the (coherent and incoherent) plasmon–exciton interactions.^[50,59] In our case, the decrease of UPR–LPR frequency difference as a function of t_2 can be modeled with an exponential decay characterized by a time constant of 40 fs.

Other investigations on the ultrafast relaxation dynamics of polariton and plexciton systems have revealed a time-dependent behavior of Ω_R , mainly explained in terms of Rabi contraction.^[17,20,22,50,59,60] This effect can be phenomenologically described, considering that photoexcitation reduces the number of ground-state molecules effectively coupled to the plasmon. As Ω_R is proportional to the square root of this number, it diminishes within the lifetime of the exciton population; and then, it recovers to the initial value in hundreds of fs timescale. The typical spectroscopic signature of this phenomenon is the appearance of dispersive lineshapes for the main peaks, manifested in the 2D maps with the presence of a negative feature in between the two diagonal signals which affects their maxima position over time.^[20] The typical extent of the contraction is a few % of the initial value.^[17,20,22,50] The trend in Figure 3 captures a different behavior. Except for the first ten fs, the peaks in the 2D maps do not have clear dispersive lineshapes. Moreover, a significant

reduction of Ω_R is recorded in the timescale of our experiment, with a decrease of over 60% in the first 100 fs. This evidence thus suggests that the predominant nonlinearity generating these ultrafast dynamics has a different physical origin, as discussed later.

Focusing now on the off-diagonal peaks, it is clear that they appear immediately after photoexcitation at crossed symmetric positions with respect to the diagonal and their dynamic evolution is completely different from the one of the diagonal peaks. The appearance of cross peaks is typically connected with couplings between excited states^[28,39,61] and as such, their presence could represent evidence for cross-interactions between the two plexciton branches, as recently proposed for a polaritonic microcavity system in the IR region.^[15,16] In this case, it is expected that the dynamics of the cross peaks along the population time t_2 reflect the time evolution of the interaction, including the presence of beatings lasting until the UPR–LPR superposition remains coherent.^[61] In addition, in strongly coupled systems, cross peaks might also appear as a mere consequence of a common ground state. Indeed, when two transitions share a common state, then pumping one of these transitions will instantaneously bleach also the other. In this case, diagonal and cross-peaks will show the same dynamics and no oscillations will be detected.^[62,63] Therefore, these two phenomena, while contributing to the signal at the same cross-coordinates, give rise to different dynamics; and

therefore, their contributions can be untangled by studying the time evolution of the signal (see also Figure S4, Supporting Information).

In light of this, the analysis of the dynamic behavior of the signal in the 2D maps at different coordinates assumes crucial importance. This analysis has been carried out by applying the global fitting methodology introduced before for the uncoupled systems. It was found that the overall evolution of the transient signal in the 2DES maps is driven by three time components: a fast decay with a time constant of ≈ 15 fs, a slower component of ≈ 55 fs, and a long time component that remains constant up to 400 fs. The amplitude distribution of these kinetics components across the 2DES maps is reported in the form of 2D-DAS (two dimensional decay associated spectra,^[42] Figure 3c–e). The sign and the position of signals appearing in the 2D-DAS provide information on the nature of the relaxation pathways and on the states mainly involved in the dynamic process characterized by that time constant. A positive (negative) amplitude in a DAS means that the signal is exponentially decaying (rising) with the related time constant.^[42,64]

The first component (15 fs) spans the same time window as the shortest dynamics found in the non-functionalized NUs (≤ 10 fs; Figure 2; Figure S9, Supporting Information). However, the corresponding DAS plots (Figure 3c for the nanohybrids; Figure S9, Supporting Information, for the NUs), are significantly different in terms of peaks' position, amplitude distribution, and sign. This evidence suggests that the ultrafast dynamics quantified by the 15 fs kinetic constant in the plexciton nanohybrids cannot be attributed to processes involving only the plasmonic moieties.

Indeed, the positive (red) peaks appearing at coordinates corresponding to the two diagonal and the two off-diagonal peaks witness a simultaneous ultrafast decay of the overall 2D map. It is also worth noticing that this is the dominant component for the cross peaks, while for the diagonal ones, longer components are more relevant (see also Figure S5, Supporting Information). These dynamics are attributed to the ultrafast dephasing of the coherent superposition of the plexcitonic states instantaneously prepared by the exciting pulses (Figure 3f). This interpretation would imply the establishment of coherent interactions between plexcitons, which, as discussed before, should lead to the presence of quantum beatings in the signal amplitude at cross-peak positions. These beatings were effectively captured and will be addressed in the next section.

The second time constant of 55 fs has a DAS dominated by a strong negative (rising) signal at an emission frequency of $\approx 17\,000\text{cm}^{-1}$, in between LPR and UPR, and a broad range of excitation frequencies (Figure 3d). This DAS captures the progressive increase of signal amplitude at an emission coordinate in between the two plexciton resonances in a sub-100 fs timescale. It also explains the reduction of the frequency gap between UPR and LPR in the same timescale as represented in Figure 3b: the two main diagonal peaks seem to get closer over time due to the effect of the growth of this signal at intermediate frequencies. The time constants are also very similar (40 and 55 fs for Figures 3b and 3d, respectively). Therefore, the results in Figure 3b,d are two different representations of the same non-linearity, whose origin can be deduced from the signal distribution in the DAS. Indeed, the horizontally elongated negative peak dominating the DAS in Figure 3d indicates a transfer of excitation

density from the states initially populated by the pulse to states falling at $17\,000\text{cm}^{-1}$, most likely dark states having the same frequency as the molecular excitons. We thus attribute these dynamics mainly to the localization of the excitation on molecular-like dark states (Figure 3g). The transfer of energy from plexciton states, especially from UPR, to dark states in hundreds of fs or less has already been observed in other systems.^[20,65–67] Here, we observe a transfer from both UPR and LPR, as witnessed by the broad range of excitation frequencies characterizing the negative blue feature in the DAS of Figure 3d. These findings agree well with recent observations suggesting that the redistribution of the population between UPR and LPR is strongly affected by the presence of a dense manifold of dark and bright states in between them, including plasmon resonances of the bare nanoparticle moieties.^[24,60,68,69] In addition to that, one should consider that the exciting pulse, together with plexcitons, can also directly excite the plasmon resonance of the NUs' moiety. As described before, after photoexcitation, plasmons might undergo redshift and broadening even when J-aggregates are present on the nanoparticle surface. This transient change in the plasmon resonance can affect the plasmon-exciton detuning and the Rabi splitting, contributing to the trend shown in Figure 3b. Although the comparison with bare NUs suggests that this process should be activated in a slightly longer timescale (≈ 125 fs, see Figure S9, Supporting Information), its contribution cannot be completely ruled out, and the current analysis does not enable the different mechanisms to be distinguished from one another.

The time constant and the signal amplitude distribution associated with this relaxation process overlap with the typical signatures expected for Rabi contraction and hinder the identification of their possible contribution. Thus, while the presence of Rabi contraction cannot be excluded, it surely does not represent the main contribution to the behavior of the nanohybrids in the current experimental conditions.

Last, the DAS associated with the longest time constant (>400 fs, Figure 3e) captures all the processes that cause a decay of the transient signal in a timescale longer than the investigated time window, including the final relaxation to the ground state (Figure 3h). Interestingly, this DAS presents a residual non-negligible signal amplitude also at cross coordinates. While the majority of the intensity at non-diagonal positions decays with the first shorter ultrafast time constant, the presence of this residual signal amplitude evolving with the same dynamics of the diagonal peaks might suggest that the transitions giving rise to the two diagonal peaks are still coupled through a common ground state. This implies that, to a certain extent, excitons and plasmons are still coupled strongly enough; plexciton states are still eigenstates for the system; and therefore, the excitation is still shared among the plasmon and the molecular moieties, at least within the duration of the investigated time window (400 fs).

2.3.2. Coherent Dynamics and Beatings Analysis

The presence of coherent dynamics in the 2DES response is manifested as beating in the signal amplitude as a function of t_2 .^[61] We are particularly interested in the possible presence of beatings at cross-peak positions because this would represent the embodiment of coherent interactions between the two plexciton

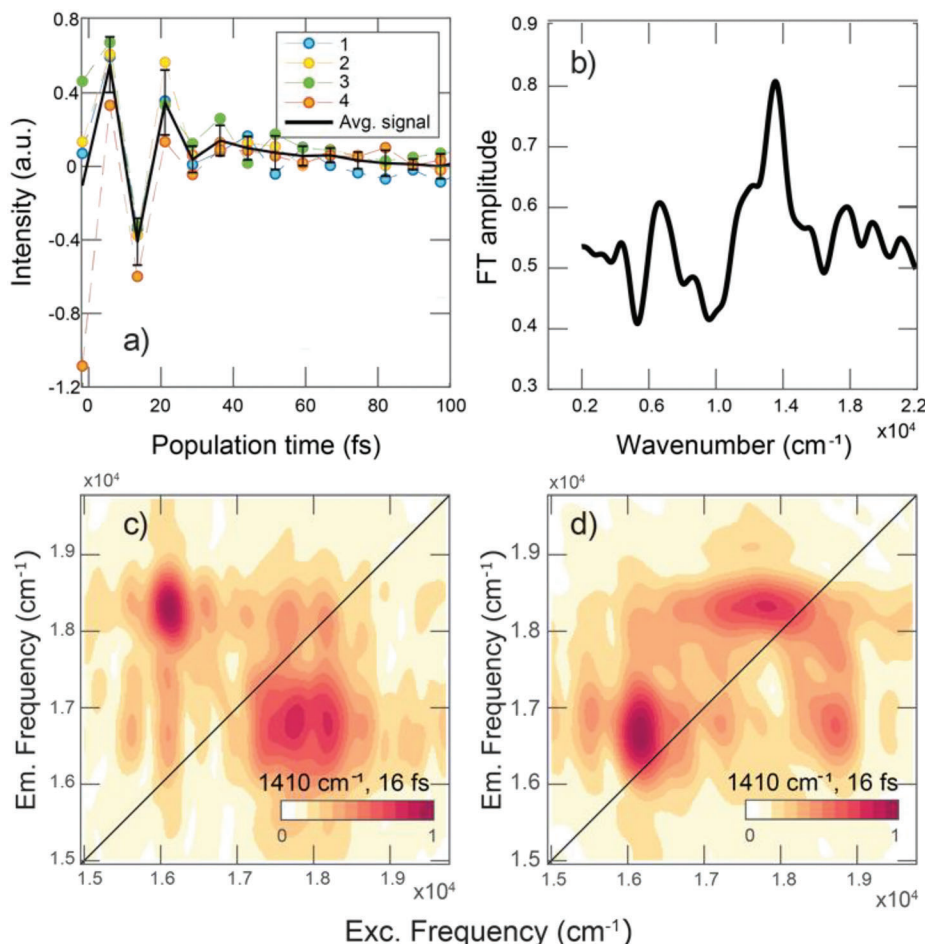


Figure 4. Beating analysis in the 2DES response of nano hybrids. a) Purely absorptive signal decays extracted at coordinates (16 200, 17 900 cm^{-1} , cyan circle in Figure 3a) in four different sets of measurements (thin colored lines) and their average (thick black line). b) Power spectrum of the beatings in the purely absorptive 2DES signal of nano hybrids. c) Normalized amplitude distribution map (absolute value 2D-CAS^[42]) obtained from the global fitting of the rephasing signal relative to the oscillation with central frequency 1410 cm^{-1} and damping time 16 fs. d) Same as (c) for the non-rephasing signal.

branches. As an example, **Figure 4a** reports the signal amplitude at the upper diagonal cross peak (cyan circle in Figure 3a at coordinates 16 200, 17 900 cm^{-1}) in four different sets of measurements and their average. The data confirm the presence of reproducible quickly damped oscillations.

The quickest way of analyzing the beating behavior of the 2DES signals is by performing a Fourier spectrum of coherences or power spectrum.^[70–72] The power spectrum is obtained by Fourier transforming the 2DES maps over t_2 after integration over the excitation and emission frequencies. Therefore, the spectrum captures the main components contributing to the overall beating behavior of the whole 2D maps. The power spectrum relative to the purely absorptive 2DES data of the nano hybrids is reported in Figure 4b, where a clear signal at $\approx 1400 \text{ cm}^{-1}$ is emerging above the noise threshold.

A more detailed picture can be extracted from the same global fitting analysis applied before, which can also provide information on the frequency, amplitude distribution, and time evolution of the beatings.^[42] The fitting correctly identified the presence of a beating component at 1410 cm^{-1} characterized by a

damping time of 16 fs. The distribution of this coherent sub-100 fs signature in the 2DES maps can be visualized in the form of 2D-CAS (two dimensional coherence-associated spectra), analogous to the previously discussed 2D-DAS. The signal distribution in the 2D-CAS is strongly dependent on the nature of the states involved in the coherent superposition whose evolution in time gives rise to that specific beating component. Specific protocols exist to assess the nature of this coherence, mainly based on the comparison between the signal amplitude in the rephasing and non-rephasing portion of the signal.^[61,73] In our case, the CAS associated with the 1410 cm^{-1} beating component shows significant amplitude only at cross-peak positions in the rephasing data (Figure 4c) and at diagonal positions in the non-rephasing spectra (Figure 4d). This is a very peculiar signal distribution typical for coherent superpositions of two electronic states,^[28,61,73,74] which further supports the attribution of the beatings to an LPR-UPR cross-interaction.

This attribution is also supported by the central frequency of the beatings that agrees well with the initial value of the frequency difference between UPR and LPR (Ω_R). Indeed, if the beatings

represent the time evolution of a coherent superposition of UPR and LPR, their oscillation frequency must correspond to the frequency difference between the two states.

Furthermore, the dephasing time of this coherent beating follows the same timescale captured by the first ultrafast time decay component, previously attributed to the loss of coherence of the initially photogenerated coherent plexcitons. It is also important to highlight that; although this dephasing time is very short, the well-defined signal distribution, the specific frequency, the reproducibility across different experiments, and the absence of similar features in the control samples rule out dominating contributions by pulse overlap artifacts.

3. Discussion

The abovementioned findings clearly highlighted that the ultrafast dynamics in the studied colloidal nano hybrids are initially driven by coherent interactions, followed by photoinduced incoherent population relaxation processes.

Indeed, it is possible to clearly distinguish a time range, covering about the first 40–50 fs after photoexcitation, during which the system evolves as a coherent superposition of UPR and LPR. This coherent regime is witnessed by the presence of significant off-diagonal signals at cross coordinates with respect to the diagonal UPR and LPR signals and by beatings in the signal amplitude, characterized by a well-defined frequency corresponding exactly to the separation between the two states. We found that the dephasing time of the coherent beatings matches the kinetic constant dominating the decay of cross-peaks, supporting the common origin and the interpretation of these two observables. So far, evidence for coherent dynamics in exciton polaritonic systems in the Vis range has been reported only in the case of solid-state systems built on ordered nanoslits arrays.^[17] A recent study performed, applying 2DES to colloidal plexcitonic nanoparticles made by TDBC J-aggregates assembled on Ag nanoprisms, estimated a dephasing time for coherent phenomena in the order of 1.7–16 fs based on absorption bandwidths, but no direct observation of coherent beating was reported.^[20] In that case, the detuning between the plasmon and the exciton resonances leads to an overestimation of the Rabi splitting and of the coupling regime, which should instead be placed in the intermediate regime (i.e., on the border of Fano interference and strong coupling leading to plexcitonic states^[75,76]) because the condition $2\Omega_R > \gamma_{\text{TDBC}} + \gamma_{\text{NUs}}$ was not fulfilled. The effective formation of coherent plexciton states was clearly a necessary condition to capture the beatings and measure a direct manifestation of coherent dynamics, but this condition was particularly arduous to be achieved with colloidal plasmonic nanoparticles, characterized by high values of dephasing rates γ . Indeed, high values of γ require high values of Ω_R in order to achieve the $2\Omega_R > \gamma_{\text{TDBC}} + \gamma_{\text{NUs}}$ inequality. On the one side, this leads to more demanding experimental coupling conditions between nanoparticles and dyes; in our case, despite their high γ , NUs are particularly suited to establish strong coupling with dyes because of the strong field enhancement effect at the tips.^[32] On the other side, considering that the coherent beating frequency corresponds to the frequency gap between the two plexcitonic branches (i.e., Ω_R), high values of Ω_R require very demanding time resolution to resolve the beatings, and this explains why conventional pump and probe measurements with

100 fs time resolution so far failed to capture coherent dynamics in these colloidal systems. These considerations confirm that the coherent regime is particularly elusive to be caught in colloidal nano hybrids and that a careful design of the nano hybrids and suitable time resolutions are needed to unveil coherent behaviors.

To further support this claim, we prepared and analyzed other samples of NUs-based plexcitonic nanoparticles where, by modulating the dye concentration during the nano hybrids preparation, an intermediate coupling regime where $2\Omega_R < \gamma_{\text{TDBC}} + \gamma_{\text{NUs}}$, was achieved, similar to what was obtained in ref. [20]. The results, summarized in Note S3 and Figures S10–S12, Supporting Information, confirm that the dynamics in these cases are dominated by incoherent processes, including relaxation from UPR to dark states and to LPR, in agreement with previous literature.^[20] As predicted for samples in the intermediate regime, for these systems, the 2DES response does not present signatures for quickly decaying cross peaks nor are quickly damped beatings ascribable to coherent dynamics of an LPR-UPR superposition.

Coming back to the strongly coupled systems, after the first 40–50 fs, the coherent interaction between plexcitons gets damped concomitantly with the progressive appearance of an incoherent relaxation phenomenon that localizes population into states falling at a frequency intermediate between UPR and LPR, most likely exciton-like dark states (Figure 3d,g). This result agrees with other recent works suggesting that the presence of a rich manifold of dark or bright states in between UPR and LPR strongly affects the relaxation dynamics of nano hybrids in the hundreds fs time range. Indeed, it was recently proposed that for exciton–polariton microcavity systems, the presence of intermolecular couplings or differences in bandgaps originates manifolds of closely spaced, non-degenerate dark or bright eigenstates in between UPR and LPR, which cascade energy.^[60] Analogously, for colloidal nano hybrids, it was demonstrated that the presence of a reservoir of intermediate energy states causes a redistribution of the population among UPR and LPR.^[8,24] These findings challenge the conventional picture of two well separated and independent UPR and LPR branches and call for more attention to the description of the manifolds of eigenstates emerging at intermediate energies between them as a consequence of the energetic disorder of the individual chromophores and the couplings among them and with the plasmonic nanoparticles.

4. Conclusion

The characterization of the ultrafast dynamics of colloidal plexciton materials is a necessary achievement to allow their effective application in quantum-nano-photonics but has remained ambiguous in the current state of the field because of the challenging nature of this task. In particular, coherent dynamics have never been captured in solutions of colloidal plexcitonic nano hybrids. Here we report the first direct experimental observation of the coherent dynamic behavior of plexcitonic resonances in water solutions of colloidal nano hybrids built by coupling gold nanourchins and J-aggregates of the molecular dye TDBC. To this aim, we took advantage of the well-known sensitivity of 2DES to dynamics of coupled states and coherent dynamics.

Solid experimental proofs of ultrafast coherent dynamics among plexciton branches were measured in nano hybrids de-

signed to achieve the so-called “strong coupling” conditions between the plasmonic and the molecular moieties. The comparison with the optical response measured for the uncoupled components further supported the pivotal role of fulfilling this regime necessary for the formation of hybrid plexcitonic states.

Overall, these results represent an important piece of information toward a more thorough comprehension and the possible control of the mechanisms regulating the ultrafast coherent dynamics in such nanohybrids and toward the development of quantum technologies where the establishment of plexciton resonances can be effectively exploited to modulate the dephasing of quantum coherence.

5. Experimental Section

Synthesis of Gold NUs and Preparation of Plexcitonic Nanohybrids: Citrate-capped gold NUs were prepared by following a modified procedure^[31] as previously described.^[5] TDBC (5,6-Dichloro-2-[[5,6-dichloro-1-ethyl-3-(4-sulfobutyl)-benzimidazol-2-ylidene]-propenyl]-1-ethyl-3-(4-sulfobutyl) benzimidazolium hydroxide, inner salt, sodium salt) was purchased by Few Chemicals and used without further purification. Nanohybrids were prepared by adding 200 μL of a 1 mM TDBC solution (J -aggregates form at this concentration) to 400 μL solution of NUs, which had a plasmon peak extinction of value 0.3 (the optical path of the cuvette was 1 mm), corresponding to an estimated concentration of ≈ 40 nm. The solution was left reacting overnight; and the day after, gently sonicated before measurements.

TEM Measurements and Extinction Spectra: TEM analysis was performed with a Jeol 300 PX electron microscope and the collected images were analyzed with ImageJ software. A detailed procedure for the calculation of NUs diameters was reported previously.^[5] The error associated with the reported diameter values is the half-width-at-half-maximum of the Gaussian fit (Figure S1, Supporting Information). Extinction spectra were recorded with a Cary 5000 spectrophotometer.

Measurements: 2DES measurements were performed in the fully non-collinear BOXCARs (photon echo) geometry using a previously described setup.^[77] Briefly, the output of an 800 nm, 3 kHz Ti:Sapphire laser system (Coherent Libra) was converted into a broad visible pulse in a non-collinear optical amplifier (Light Conversion TOPAS White). The transform-limited condition for the pulses at the sample position was achieved through a prism compressor coupled with a Fastlite Dazzler pulse shaper for fine adjustment. The 2DES experiment relied on the passively phase stabilized setup, where the laser output was split into four identical phase-stable beams (three exciting beams and a fourth beam further attenuated of three orders of magnitude and used as Local Oscillator, LO) in a BOXCARs geometry using a suitably designed 2D grating. Pairs of four CaF_2 wedges modulate time delays between pulses. One wedge of each pair was mounted onto a translation stage (Aerotech ANT-95) that regulated the thickness of the medium crossed by the exciting beam and provided a temporal resolution of 0.07 fs. Delay times t_1 (coherence time between first and second exciting pulse), t_2 (population time between second and third exciting pulse), and t_3 (rephasing time between the third exciting pulse and the emitted signal) were defined. The rephasing and non-rephasing parts of the signal could be recorded by acting on the pulse sequence. The purely absorptive signal was then calculated as the sum of the rephasing and non-rephasing signals.^[77] The outcome of the experiment was a 3D array of data describing the evolution of 2D frequency–frequency (rephasing, non rephasing or purely absorptive) correlation maps as a function of t_2 . In each map, the excitation and emission frequency axes were obtained by Fourier transforming t_1 and t_3 , respectively.

The laser spectrum was centered at $17\,390\text{ cm}^{-1}$ (575 nm) to cover both plexcitonic branches. The pulse duration, optimized through FROG measurements, was compressed down to 10 fs, corresponding to a spectral bandwidth of $\approx 3330\text{ cm}^{-1}$ (Figure S6, Supporting Information). t_2 was

scanned from 0 to 400 fs with steps of 7.5 fs while the coherence time (t_1) from 0 to 125 fs was in steps of 3 fs. The energy of the pulse at the sample position was set to ≈ 5 nJ per pulse. For each sample, measurements were repeated three times to guarantee reproducibility. Steady-state absorption spectra were acquired before and after each scan to control that no sample degradation had occurred during the 2DES measurements.

Supporting Information

Supporting Information is available from the Wiley Online Library or from the author.

Acknowledgements

This research is funded by the P-DiSC#04BIRD2022-UNIPD Grant. The “CQ-TECH” STARS Grant 2019 (2019-UNPD0Z9- 0166571) is also acknowledged. The authors gratefully thank Prof. Stefano Corni for insightful discussions and Elisa Fresch and Giampaolo Marcolin for technical support with 2DES experiments.

Conflict of Interest

The authors declare no conflict of interest.

Data Availability Statement

The data that support the findings of this study are available from the corresponding author upon reasonable request.

Keywords

2D electronic spectroscopy, coherent dynamics, colloidal nanoparticles, light–matter coupling, plasmons, plexcitons, polaritons

Received: December 15, 2022

Revised: March 30, 2023

Published online:

- [1] N. Rivera, I. Kaminer, *Nat. Rev. Phys.* **2020**, *2*, 538.
- [2] H. M. Gibbs, G. Khitrova, S. W. Koch, *Nat. Photonics* **2011**, *5*, 273.
- [3] D. G. Baranov, M. Wersäll, J. Cuadra, T. J. Antosiewicz, T. Shegai, *ACS Photonics* **2018**, *5*, 24.
- [4] P. Törmä, W. L. Barnes, *Rep. Prog. Phys.* **2015**, *78*, 013901.
- [5] N. Peruffo, F. Mancin, E. Collini, *J. Phys. Chem. C* **2021**, *125*, 19897.
- [6] B. Kolaric, B. Maes, K. Clays, T. Durt, Y. Caudano, *Adv. Quantum Technol.* **2018**, *1*, 1800001.
- [7] N. Peruffo, G. Parolin, E. Collini, S. Corni, F. Mancin, *Nanomaterials* **2022**, *12*, 1180.
- [8] N. Peruffo, G. Gil, S. Corni, F. Mancin, E. Collini, *Nanoscale* **2021**, *13*, 6005.
- [9] E. Cao, W. Lin, M. Sun, W. Liang, Y. Song, *Nanophotonics* **2018**, *7*, 145.
- [10] M. Hertzog, M. Wang, J. Mony, K. Börjesson, *Chem. Soc. Rev.* **2019**, *48*, 937.
- [11] A. P. Manuel, A. Kirkey, N. Mahdi, K. Shankar, *J. Mater. Chem. C* **2019**, *7*, 1821.
- [12] D. Brinks, M. Castro-Lopez, R. Hildner, N. F. van Hulst, *Proc. Natl. Acad. Sci. U. S. A.* **2013**, *110*, 18386.

- [13] M. S. Tame, K. R. McEnery, Ş. K. Özdemir, J. Lee, S. A. Maier, M. S. Kim, *Quantum Plasmonics*, Springer International Publishing, Cham, Switzerland **2013**.
- [14] D. Xu, X. Xiong, L. Wu, X.-F. Ren, C. E. Png, G.-C. Guo, Q. Gong, Y.-F. Xiao, L. In, X. En, C. Ng, G. Uo, Q. Ong, Y. Iao, *Adv. Opt. Photonics* **2019**, *10*, 703.
- [15] N. Takemura, S. Trebaol, M. D. Anderson, V. Kohnle, Y. Léger, D. Y. Oberli, M. T. Portella-Oberli, B. Deveaud, *Phys. Rev. B: Condens. Matter Mater. Phys.* **2015**, *92*, 125415.
- [16] B. Xiang, R. F. Ribeiro, L. Chen, J. Wang, M. Du, J. Yuen-Zhou, W. Xiong, *Sci. Adv.* **2021**, *5*, eaax5196.
- [17] P. Vasa, W. Wang, R. Pomraenke, M. Lammers, M. Maiuri, C. Manzoni, G. Cerullo, C. Lienau, *Nat. Photonics* **2013**, *7*, 128.
- [18] S. Takahashi, K. Watanabe, *J. Phys. Chem. Lett.* **2020**, *11*, 1349.
- [19] L. Mewes, M. Wang, R. A. Ingle, K. Börjesson, M. Chergui, *Commun Phys* **2020**, *3*, 157.
- [20] D. Finkelstein-Shapiro, P.-A. Mante, S. Sarisozen, L. Wittenbecher, I. Minda, S. Balci, T. Pullerits, D. Zigmantas, *Chem* **2021**, *7*, 1092.
- [21] N. T. Fofang, N. K. Grady, Z. Fan, A. O. Govorov, N. J. Halas, *Nano Lett.* **2011**, *11*, 1556.
- [22] T. Simon, D. Melnikau, A. Sánchez-Iglesias, M. Grzelczak, L. M. Liz-Marzán, Y. Rakovich, J. Feldmann, A. S. Urban, *J. Phys. Chem. C* **2016**, *120*, 12226.
- [23] S. Balci, C. Kocabas, B. Küçüköz, A. Karatay, E. Akhüseyin, H. Gul Yaglioglu, A. Elmali, *Appl. Phys. Lett.* **2014**, *105*, 051105.
- [24] N. Peruffo, F. Mancin, E. Collini, *J. Phys. Chem. Lett.* **2022**, *13*, 6412.
- [25] K. M. Pelzer, G. B. Griffin, S. K. Gray, G. S. Engel, *J. Chem. Phys.* **2012**, *136*, 164508.
- [26] G. Nardin, G. Moody, R. Singh, T. M. Autry, H. Li, F. Morier-Genoud, S. T. Cundiff, *Phys. Rev. Lett.* **2014**, *112*, 46402.
- [27] E. Collini, H. Gattuso, E. Kolodny, L. Bolzonello, A. Volpato, H. T. Fridman, S. Yochelis, M. Mor, J. Dehnell, E. Lifshitz, Y. Paltiel, R. D. Levine, F. Remacle, *J. Phys. Chem. C* **2020**, *124*, 16222.
- [28] E. Collini, *J. Phys. Chem. C* **2021**, *125*, 13096.
- [29] G. Moody, S. T. Cundiff, *Adv. Phys. X* **2017**, *2*, 641.
- [30] Y. Kobayashi, Ed., *J-Aggregates*, World Scientific, Singapore, **1996**.
- [31] J. Li, J. Wu, X. Zhang, Y. Liu, D. Zhou, H. Sun, H. Zhang, B. Yang, *J. Phys. Chem. C* **2011**, *115*, 3630.
- [32] P. Senthil Kumar, I. Pastoriza-Santos, B. Rodríguez-González, F. Javier García De Abajo, L. M. Liz-Marzán, *Nanotechnology* **2008**, *19*, 015606.
- [33] T. W. Ebbesen, *Acc. Chem. Res.* **2016**, *49*, 2403.
- [34] J. Flick, N. Rivera, P. Narang, *Nanophotonics* **2018**, *7*, 1479.
- [35] J. T. Hugall, A. Singh, N. F. van Hulst, *ACS Photonics* **2018**, *5*, 43.
- [36] P. Törmä, W. L. Barnes, *Rep. Prog. Phys.* **2014**, *78*, 013901.
- [37] D. Melnikau, P. Samokhvalov, A. Sánchez-Iglesias, M. Grzelczak, I. Nabiev, Y. P. Rakovich, *J. Lumin.* **2022**, *242*, 118557.
- [38] E. Fresch, N. Peruffo, M. Trapani, M. Cordaro, G. Bella, M. A. Castriciano, E. Collini, *J. Chem. Phys.* **2021**, *154*, 084201.
- [39] A. Gelzinis, R. Augulis, V. Butkus, B. Robert, L. Valkunas, *Biochim. Biophys. Acta Bioenergetics* **2019**, *1860*, 271.
- [40] M. Van Burgel, D. A. Wiersma, K. Duppen, *J. Chem. Phys.* **1995**, *102*, 20.
- [41] L. Lüer, S. K. Rajendran, T. Stoll, L. Ganzer, J. Rehault, D. M. Coles, D. Lidzey, T. Virgili, G. Cerullo, *J. Phys. Chem. Lett.* **2017**, *8*, 547.
- [42] A. Volpato, L. Bolzonello, E. Meneghin, E. Collini, *Opt. Express* **2016**, *24*, 24773.
- [43] J. H. Lee, C. K. Min, T. Joo, *J. Chem. Phys.* **2001**, *114*, 377.
- [44] K. Minoshima, M. Taiji, K. Misawa, T. Kobayashi, *Chem. Phys. Lett.* **1994**, *218*, 67.
- [45] J. Moll, S. Daehne, J. R. Durrant, D. A. Wiersma, *J. Chem. Phys.* **1995**, *102*, 6362.
- [46] S. Link, M. A. El-Sayed, *J. Phys. Chem. B* **1999**, *103*, 4212.
- [47] C. Sönnichsen, T. Franzl, T. Wilk, G. von Plessen, J. Feldmann, O. Wilson, P. Mulvaney, *Phys. Rev. Lett.* **2002**, *88*, 774021.
- [48] G. v Hartland, *Chem. Rev.* **2011**, *111*, 3858.
- [49] A. Liétard, C. S. Hsieh, H. Rhee, M. Cho, *Nat. Commun.* **2018**, *9*, 891.
- [50] Y. Tang, Y. Zhang, Q. Liu, K. Wei, X. Cheng, L. Shi, T. Jiang, *Light: Sci. Appl.* **2022**, *11*, 94.
- [51] D. A. Wheeler, T. D. Green, H. Wang, C. Fernández-López, L. Liz-Marzán, S. Zou, K. L. Knappenberger, J. Z. Zhang, *Chem. Phys. Lett.* **2012**, *543*, 127.
- [52] W. R. Jeffries, K. Park, R. A. Vaia, K. L. Knappenberger, *Nano Lett.* **2020**, *20*, 7722.
- [53] G. v Hartland, *Annu. Rev. Phys. Chem.* **2006**, *57*, 403.
- [54] M. E. Siemens, G. Moody, H. Li, A. D. Bristow, S. T. Cundiff, *Opt. Express* **2010**, *18*, 17699.
- [55] E. W. Knapp, *Chem. Phys.* **1984**, *85*, 73.
- [56] J. Knoester, *Chem. Phys. Lett.* **1993**, *203*, 371.
- [57] M. Wurdack, E. Estrecho, S. Todd, T. Yun, M. Pieczarka, S. K. Earl, J. A. Davis, C. Schneider, A. G. Truscott, E. A. Ostrovskaya, *Nat. Commun.* **2021**, *12*, 53666.
- [58] R. Houdré, R. P. Stanley, M. Ilegems, *Phys. Rev. A: At., Mol., Opt. Phys.* **1996**, *53*, 2711.
- [59] P. Vasa, R. Pomraenke, G. Cirmi, E. de Re, W. Wang, S. Schwieger, D. Leipold, E. Runge, G. Cerullo, C. Lienau, *ACS Nano* **2010**, *4*, 7559.
- [60] M. Son, Z. T. Armstrong, R. T. Allen, A. Dhavamani, M. S. Arnold, M. T. Zanni, *Nat. Commun.* **2022**, *13*, 7305.
- [61] E. Collini, *Chem. Soc. Rev.* **2013**, *42*, 4932.
- [62] E. Cassette, J. C. Dean, G. D. Scholes, *Small* **2016**, *12*, 2234.
- [63] M. Righetto, L. Bolzonello, A. Volpato, G. Amoruso, A. Panniello, E. Fanizza, M. Striccoli, E. Collini, *Phys. Chem. Chem. Phys.* **2018**, *20*, 18176.
- [64] I. H. M. van Stokkum, D. S. Larsen, R. van Grondelle, *Biochim. Biophys. Acta Bioenergetics* **2004**, *1657*, 82.
- [65] R. F. Ribeiro, L. A. Martínez-Martínez, M. Du, J. Campos-Gonzalez-Angulo, J. Yuen-Zhou, *Chem. Sci.* **2018**, *9*, 6325.
- [66] D. G. Lidzey, A. M. Fox, M. D. Rahn, M. S. Skolnick, V. M. Agranovich, S. Walker, *Phys. Rev. B: Condens. Matter Mater. Phys.* **2002**, *65*, 195312.
- [67] T. Virgili, D. Coles, A. M. Adawi, C. Clark, P. Michetti, S. K. Rajendran, D. Brida, D. Polli, G. Cerullo, D. G. Lidzey, *Phys. Rev. B: Condens. Matter Mater. Phys.* **2011**, *83*, 2.
- [68] G. D. Scholes, C. A. Delpo, B. Kudisch, *J. Phys. Chem. Lett.* **2020**, *11*, 6389.
- [69] G. Groenhof, C. Climent, J. Feist, D. Morozov, J. J. Toppari, *J. Phys. Chem. Lett.* **2019**, *10*, 5476.
- [70] F. D. Fuller, J. Pan, A. Gelzinis, V. Butkus, S. S. Senlik, D. E. Wilcox, C. F. Yocum, L. Valkunas, D. Abramavicius, J. P. Ogilvie, *Nat. Chem.* **2014**, *6*, 706.
- [71] L. Bolzonello, A. Polo, A. Volpato, E. Meneghin, M. Cordaro, M. Trapani, M. Fortino, A. Pedone, M. A. Castriciano, E. Collini, *J. Phys. Chem. Lett.* **2018**, *9*, 1079.
- [72] E. Thyraug, C. N. Lincoln, F. Branchi, G. Cerullo, V. Perlik, F. Šanda, H. Lokstein, J. Hauer, *Photosynth. Res.* **2018**, *135*, 45.
- [73] V. Butkus, D. Zigmantas, L. Valkunas, D. Abramavicius, *Chem. Phys. Lett.* **2012**, *545*, 40.
- [74] A. M. Brańczyk, D. B. Turner, G. D. Scholes, A. M. Brańczyk, D. B. Turner, G. D. Scholes, *Ann. Phys.* **2014**, *526*, 31.
- [75] M. Pelton, S. D. Storm, H. Leng, *Nanoscale* **2019**, *11*, 14540.
- [76] F. Nan, S. J. J. Ding, L. Ma, Z. Q. Q. Cheng, Y. T. T. Zhong, Y. F. F. Zhang, Y. H. H. Qiu, X. Li, L. Zhou, Q. Q. Q. Wang, *Nanoscale* **2016**, *8*, 15071.
- [77] L. Bolzonello, A. Volpato, E. Meneghin, E. Collini, *J. Opt. Soc. Am. B* **2017**, *34*, 1223.